26 Jan 2022

AlF3-Al2O3 ALD Thin-Film-Coated Li1.2Mn0.54Co0.13Ni0.13O2 Particles for Lithium-Ion Batteries: Long-Term Protection

Han Yu

Xiaoqing He

Xinhua Liang
Missouri University of Science and Technology, liangxin@mst.edu

Recommended Citation

H. Yu et al., "AlF3-Al2O3 ALD Thin-Film-Coated Li1.2Mn0.54Co0.13Ni0.13O2 Particles for Lithium-Ion Batteries: Long-Term Protection," *ACS Applied Materials and Interfaces*, vol. 14, no. 3, pp. 3991 - 4003, American Chemical Society, Jan 2022.
The definitive version is available at https://doi.org/10.1021/acsami.1c20005

ACS APPLIED MATERIALS & INTERFACES

www.acsami.org

Research Article

AlF_3-Al_2O_3 ALD Thin-Film-Coated $Li_{1.2}Mn_{0.54}Co_{0.13}Ni_{0.13}O_2$ Particles for Lithium-Ion Batteries: Long-Term Protection

Han Yu, Xiaoqing He, and Xinhua Liang*

Cite This: *ACS Appl. Mater. Interfaces* 2022, 14, 3991−4003

Read Online

ACCESS | Metrics & More | Article Recommendations | Supporting Information

ABSTRACT: Improving the performance of existing cathode materials of lithium-ion batteries (LIBs) through surface modification has been proven to be an effective way to improve the performance of LIBs. However, it is a challenge to use a traditional method to prepare an effective coating film, which meets the requirements of uniformity, continuity, electrochemical stability, and strong mechanical properties. In this study, an ultrathin AlF_3-Al_2O_3 film was coated on the surface of $Li_{1.2}Mn_{0.54}Co_{0.13}Ni_{0.13}O_2$ (LRNMC) particles by atomic layer deposition (ALD) in a fluidized bed reactor. A cathode electrolyte interphase layer mainly composed of inorganic components was formed on the surface of AlF_3-Al_2O_3-coated LRNMC during the charge/discharge cycling process, which led to the enhancement of capacity and cycling stability. In addition, the coating layer significantly increased the shelf life of the cathode particles. For LRNMC particles with one cycle of Al_2O_3 ALD and one cycle of AlF_3 ALD coatings, there was no obvious degradation of electrochemical performance after being stored for more than 1 year, indicating long-term protection of ALD films for LIB cathode particles.

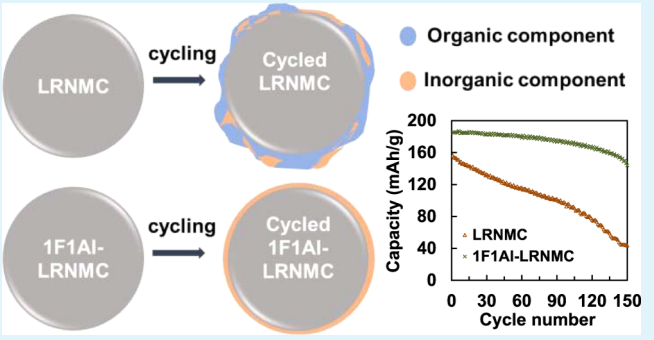

KEYWORDS: *lithium-ion battery, surface coating, atomic layer deposition, cathode electrolyte interphase, AlF_3 coating*

INTRODUCTION

More and more automobile manufacturers have stated that electric vehicles will replace traditional fuel vehicles in the next few decades. This heralds a huge room for development in the field of energy storage. As the most important energy source for electric vehicles (EVs), lithium-ion batteries (LIBs) are increasingly challenged by the requirements of higher power density and higher efficiency.[1,2] As a promising cathode material for the next generation of LIBs, Li-rich $LiTMO_2$-type layered oxides (LRTMO) can deliver discharge capacities of 250−300 mAh/g (energy density over 700 Wh/kg), which is most likely to meet the requirements of EVs.[3,4] However, the practical application of LRTMO has been hindered due to several intrinsic limitations, such as phase transition,[5] migration of transition metal ions,[6] voltage fade,[7] hysteresis,[8] impedance at low states of charge, poor rate performance, and air instability.[9]

In addition to the abovementioned problems caused by the inherent characteristics of the material, severe interface reaction between cathode and electrolyte is another thorny issue.[10] As the oxidation stability of current commercial organic carbonate solvents (e.g., ethylene carbonate (EC) and dimethyl carbonate (DMC)) is as high as 5 V vs Li^+/Li[11] and the LRTMO-based battery operates at 4.8 V, their degradation should mainly be affected by the chemical properties of the cathode surface. However, unique chemical reactions on the surface of lithium-rich electrodes, such as the release of O_2, can cause the decomposition of organic carbonates to form polymerized carbon and the decomposition of $LiPF_6$.[12] Therefore, it is particularly important to make appropriate modifications on the surface of LRTMO to inhibit this series of side reactions.

To address the interfacial issues, surface coating on cathode materials is considered one of the most effective approaches.[13,14] An effective coating should meet the following requirements: controllable film thickness, uniform and continuous coating on the substrates, and excellent electrochemical stability.[15,16] Atomic layer deposition (ALD) has the advantages of controllable thickness and uniform coating,[17,18] which can prepare films well meeting the first two requirements, while the third requirement should be considered from the performance of the coating film itself.

To meet the electrochemical stability of the interfacial layer, its electrochemical window must be wide enough to avoid decomposition due to reduction or oxidation during charge/

Received: October 16, 2021
Accepted: January 2, 2022
Published: January 13, 2022

https://doi.org/10.1021/acsami.1c20005
ACS Appl. Mater. Interfaces 2022, 14, 3991−4003

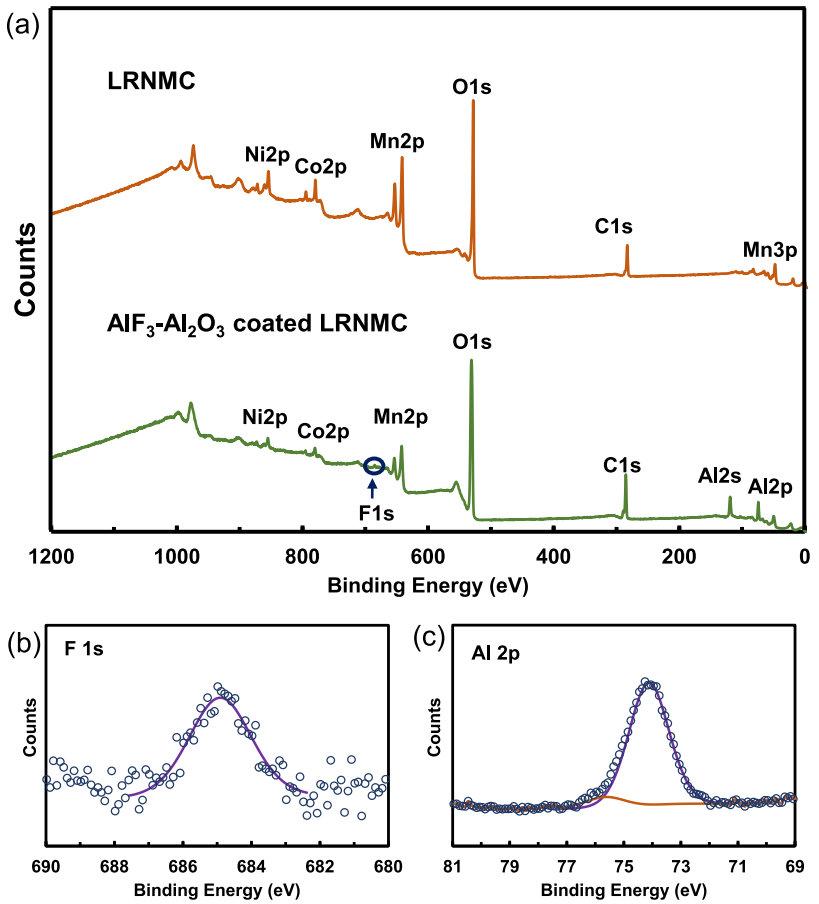

Figure 1. XPS spectra of survey scan of (a) LRNMC and AlF_3-Al_2O_3-coated LRNMC particles. High-resolution spectra of (b) F 1s and (c) Al 2p of AlF_3-Al_2O_3-coated LRNMC particles.

discharge cycling. Richards et al.[19] reported electrochemical stability windows of some candidate compounds for this purpose using the formation energy reported in some material project databases.[20] Among a series of compounds (e.g., oxides, nitrides, and phosphate), which can be used as coating materials, the electrochemical stability of fluoride is particularly prominent.[21,22] The stability window of LiF is as wide as 0−6.4 V vs Li^+/Li.[23,24] However, the low ionic and electronic conductivity of LiF are new issues. Al_2O_3 has been reported as an effective coating material on some cathode materials,[25,26] such as $LiCoO_2$, as it can effectively inhibit side reactions[27] and form ion-conducting $LiAlO_2$ on the surface of the electrode material.[28] However, the electrochemical stability window of Al_2O_3 itself vs Li^+/Li is 0.2−3.8 V; therefore it is gradually consumed during charge/discharge cycling, which is one of the reasons that it cannot provide long-term protection.[24]

In our previous research, we found that AlF_3-Al_2O_3 coated on cathode electrodes by ALD generated $LiAlF_4$ with good ionic conductivity and a wide electrochemical stability window (2.0−5.7 V vs Li^+/Li) during the cycling process, which can effectively avoid the problem of insulation and electrochemical instability.[29] It should be pointed out that ALD coating on the electrode surface directly does not block the pathway of electrons inside the electrode, and even the coating material is not conductive.[30] However, the issue is that the coating film cannot uniformly cover all of the surface of the active material; as long as part of the surface is exposed to the electrolyte, side reactions will be triggered, resulting in a decrease in electrochemical performance.[31] In contrast, conformal ALD coating on all of the surfaces of all active material particles can provide better protection, and this strategy is more suitable for practical application. In this study, we applied ALD to coat ultrathin films on Li-rich $Li_{1.2}Mn_{0.54}Co_{0.13}Ni_{0.13}O_2$ (LRNMC) particles and found that slight fluorination of Al_2O_3 coating on LRNMC particles showed much better electrochemical performance, compared to that of uncoated LRNMC particles and pure Al_2O_3 ALD coated LRNMC particles. The mechanism for the performance enhancement of AlF_3-Al_2O_3 ALD coated LRNMC particles and the composition change of cathode electrolyte interphase (CEI) were systematically studied. In addition, AlF_3-Al_2O_3-coated LRNMC showed excellent long-term protection, even after storage for over 1 year.

RESULTS AND DISCUSSION

Characterizations of ALD Coated Samples. Different thicknesses of Al_2O_3 and AlF_3 films were coated on LRNMC particles by ALD. Al_2O_3-coated LRNMC particles were denoted as *x*Al-LRNMC (*x* represents the number of ALD cycles). For fluorination of Al_2O_3, one cycle of AlF_3 was coated on Al_2O_3-coated LRNMC particles, denoted as 1F*x*Al-LRNMC. X-ray photoelectron spectroscopy (XPS) was performed to analyze the surface compositions of LRNMC particles before and after the ALD coating. XPS spectra of the survey scan of LRNMC, Al_2O_3-coated LRNMC, and AlF_3-Al_2O_3-coated LRNMC particles are shown in Figures 1 and S1a. Compared with pristine LRNMC (Figure 1a), the AlF_3-

https://doi.org/10.1021/acsami.1c20005
ACS Appl. Mater. Interfaces 2022, 14, 3991−4003

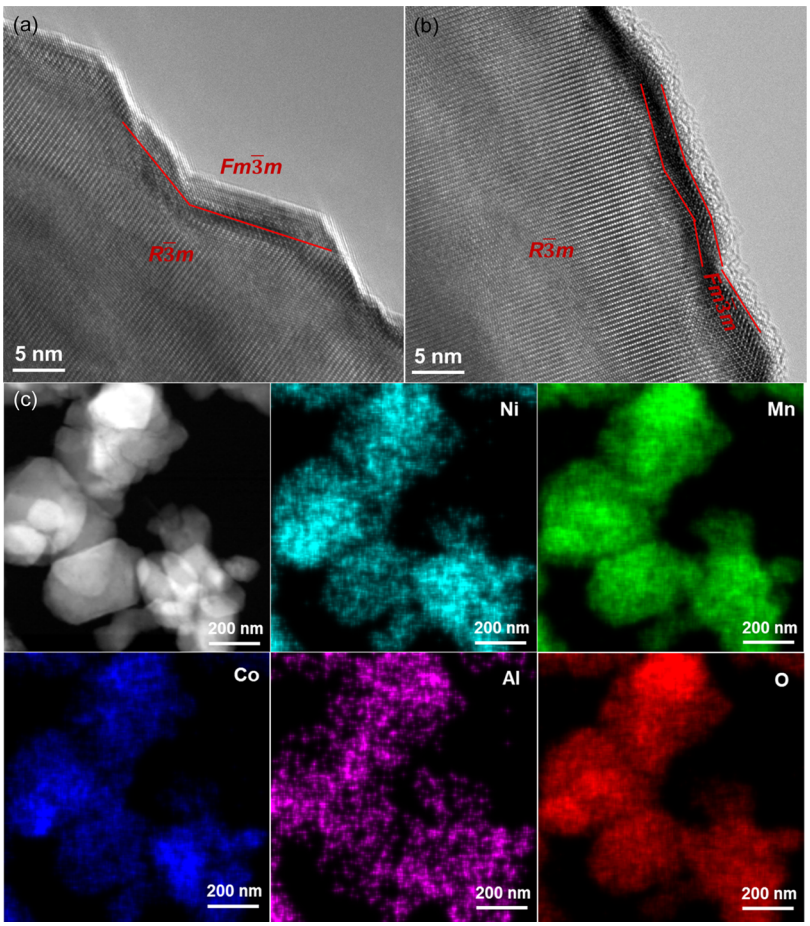

Figure 2. HRTEM images of (a) LRNMC and (b) 1F1Al-LRNMC particles and (c) EDS mapping of Ni, Mn, Co, Al, and O of 1F1Al-LRNMC particles.

Al_2O_3-coated LRNMC particles exhibited additional peaks for Al 2p, Al 1s, and F 1s, which verified the successful deposition of AlF_3 and Al_2O_3 films on the surface of the LRNMC particles by ALD. Different from the strong Al 2p and Al 1s peaks, the F 1s peak was relatively weak in the full survey scan spectrum. This was because only a pulsed dosage of HF was applied during the ALD coating process to avoid the generation of LiF due to excess HF dose. Therefore, the peak intensity of F was significantly lower than that of Al. In the high-resolution XPS spectra, a clear peak at 684.5 eV of F 1s was observed, as shown in Figure 1b. The XPS result of F 1s indicates that no LiF was generated. The Al 2p of Al_2O_3-coated LRNMC (Figure S1b) at 74.05 eV indicates that there was no other component in the Al_2O_3 ALD film. In the high-resolution Al 2p spectrum of AlF_3-Al_2O_3-coated LRNMC (Figure 1c), most of Al 2p was at 74.02 eV, with only a small part of Al 2p at 76.02 eV, which belongs to AlF_3, indicating that the main component of the coating was Al_2O_3 with only a small amount of AlF_3. This result confirms that the content of AlF_3 can be effectively controlled by controlling the dose time of HF during the ALD process.

Transmission electron microscopy (TEM) was applied to verify the thickness of the ALD film. Figure 2a shows a high-resolution transmission electron microscopy (HRTEM) image of a part of one LRNMC particle. There was a rock-salt phase ($Fm\bar{3}m$) with a thickness of about 3−4 nm on the top of the bulk layered phase ($R\bar{3}m$), without other components on the surface of LRNMC. Compared to LRNMC, the 1F1Al-LRNMC particle showed almost the same crystal structure (Figure 2b); on the top of the rock-salt phase, an amorphous film with a thickness of 1−2 nm was observed, indicating that an ultrathin AlF_3-Al_2O_3 film was coated on the surface of LRNMC particles. Figure 2c shows the energy-dispersive spectroscopy (EDS) mapping of elements Mo, Co, Ni, Al, and O of the 1F1Al-LRNMC particles. The good distribution of the Al element indicates that the ALD thin film was uniformly coated on the particle surface. Due to the overlapping of energy of Mn Lα with F Kα, and the content of Mn was much higher than that of F, no F signal was observed.

Electrochemical Performance. In our previous study,[29] we found that AlF_3-Al_2O_3 coating on cathode electrodes could form $LiAlF_4$ with good ionic conductivity and electronic conductivity during the charge/discharge cycling process, which can effectively avoid insulation problems of the coating material. However, LiF could be produced during the ALD coating process, which seriously affects the C-rate performance. Therefore, when we coat thin films on particles, it is very important to limit/avoid the formation of LiF. To achieve this, a much shorter HF dose time was applied during the ALD process. It was confirmed by XPS analysis that no LiF was generated. To study the effects of the coating on the electrochemical performance of the LRNMC particles, lithium-ion half cells were assembled by applying modified LRNMC particles as the cathode material and lithium metal as the anode. Figure 3a shows the C-rate performance of batteries based on LRNMC, Al_2O_3-coated LRNMC, and AlF_3-Al_2O_3-

https://doi.org/10.1021/acsami.1c20005
ACS Appl. Mater. Interfaces 2022, 14, 3991−4003

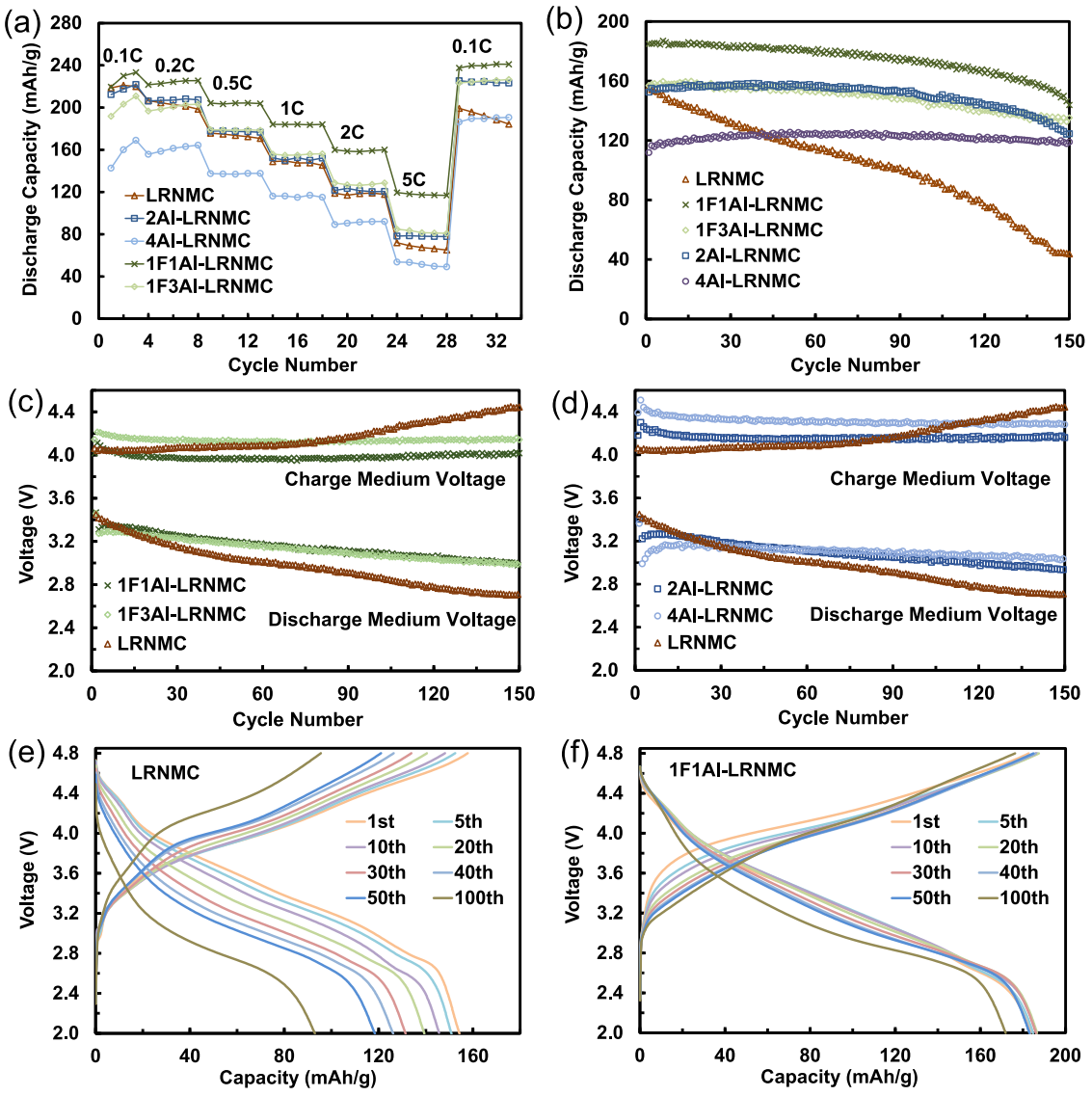

Figure 3. (a) C-rate performance and (b) discharge performance at a 1C rate of half cells made of uncoated LRNMC, AlF_3-Al_2O_3-coated LRNMC, and Al_2O_3-coated LRNMC particles. Charge and discharge medium voltages of half cells made of (c) uncoated and AlF_3-Al_2O_3-coated LRNMC particles and (d) uncoated and Al_2O_3-coated LRNMC particles. Charge/discharge profiles of half cells made of (e) LRNMC and (f) 1F1Al-LRNMC particles at various cycles during charge/discharge at a 1C rate.

coated LRNMC particles. 2Al-LRNMC delivered the same discharge capacity as LRNMC under different C rates. When the current was changed from a 5C rate back to a 0.1C rate, 2Al-LRNMC could repeat the initial performance with very good stability; however, LRNMC could not reach the initial performance, and the discharge capacity decreased during the charge/discharge process. This indicates that although Al_2O_3 coating could effectively improve its cycling stability, it could not improve the single-lap capacity of LRNMC. Compared to 2Al-LRNMC, 1F1Al-LRNMC not only improved the cycling stability of LRNMC but also improved the capacity. 1F1Al-LRNMC delivered increased discharge capacity at different C-rates, especially at a 5C rate, and the discharge capacity still reached 120 mAh/g.

Figure 3b shows the discharge performance of half cells based on LRNMC, Al_2O_3-coated LRNMC, and AlF_3-Al_2O_3-coated LRNMC particles for up to 150 cycles of charge/discharge at a 1C rate between 2.0 and 4.8 V at room temperature. LRNMC delivered an initial discharge capacity of ~156 mAh/g, but the capacity kept decreasing during the cycling process, which was due to the inherent property of this type of material and strong side reactions between electrode and electrolyte. In contrast, the ALD coated LRNMC showed quite superior cycling stability. 1F1Al-LRNMC and 2Al-LRNMC delivered the best initial discharge capacities of ~182 and ~155 mAh/g, respectively; after 100 cycles of charge/discharge, the discharge capacity of 1F1Al-LRNMC and 2Al-NMC remained at 171 and 152 mAh/g, respectively, while LRNMC was only 97 mAh/g. In general, the cycling stability could be improved with the increase of the thickness of Al_2O_3 ALD films; however, the discharge capacity decreased as a trade-off. 1F3Al-LRNMC delivered almost the same discharge performance, while the discharge capacity of 4Al-LRNMC was significantly reduced. Compared to uncoated and Al_2O_3-coated LRNMC particles, the improvement of AlF_3-Al_2O_3-coated LRNMC in both cycling stability and capacity can be attributed to the limited formation of LiF during the

https://doi.org/10.1021/acsami.1c20005
ACS Appl. Mater. Interfaces 2022, 14, 3991−4003

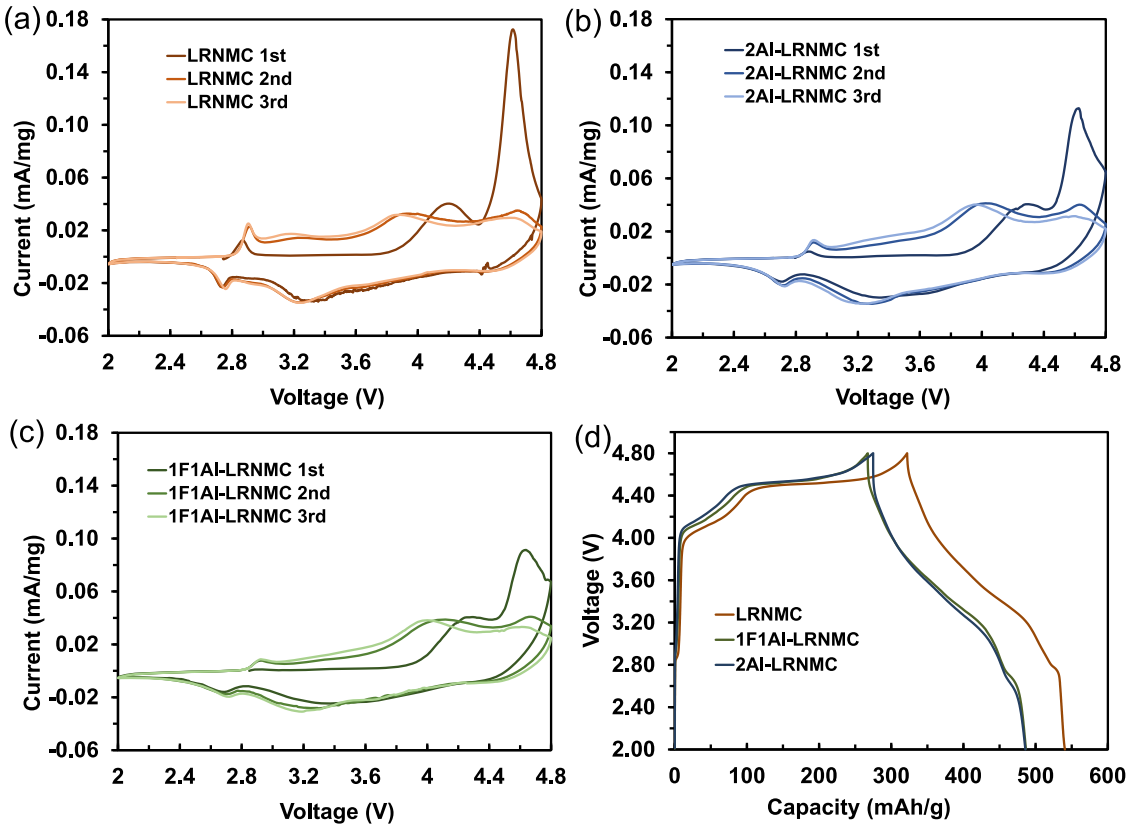

Figure 4. First three cycles of cyclic voltammograms of half cells made of (a) uncoated LRNMC, (b) 2Al-LRNMC, and (c) 1F1Al-LRNMC particles. (d) First cycle of charge/discharge profile of half cells made of uncoated LRNMC, 2Al-LRNMC, and 1F1Al-LRNMC particles.

ALD coating process and the formation of $LiAlF_4$ during the charge/discharge cycling process.

Figure 3c,d shows the charge and discharge medium voltage of half cells based on uncoated and coated LRNMC particles. LRNMC exhibited a low initial medium voltage and a high discharge medium voltage, but the voltage difference of the medium voltage gradually increased during the charge/discharge cycling, which is due to the internal structure of LRNMC gradually transferring from a layered phase to a spinel phase during the cycling process.[32,33] Compared with that of LRNMC, all coated LRNMC exhibited a slightly higher initial voltage difference, and this difference remained almost unchanged during the entire cycling process. Among them, 1F1Al-LRNMC showed the smallest voltage difference. This indicates that both Al_2O_3 coating and AlF_3-Al_2O_3 coating can inhibit the phase transition to a certain extent during the cycling process, and the performance of the AlF_3-Al_2O_3-coated LRNMC was better. Voltage capacity profiles of half cells based on LRNMC and 1F1Al-LRNMC (Figure 3e,f) showed the change of the charge/discharge platform during the cycling process more intuitively. During the first 50 cycles of charge/discharge, the voltage capacity curves of 1F1Al-LRNMC almost overlapped, while LRNMC showed an obvious trend of capacitance decrease.

The first three cycles of voltammograms of half cells made of LRNMC, 2Al-LRNMC, and 1F1Al-LRNMC, respectively, were collected at a sweep rate of 0.05 mV/s between 4.8 and 2.0 V, as shown in Figure 4a−c. For the convenience of comparison, the current of the cyclic voltammetry (CV) curves was normalized, and the same ordinate scale was used. The overall features of the CV curves for uncoated and coated LRNMC were the same in general, indicating that the coating layer did not change the inner structure of the host material. The difference between uncoated and coated LRNMC was mainly from the intensity of the highest peak between 4.6 and 4.7 V in the first cycle. Moreover, starting from the second cycle, the intensity of this peak was significantly reduced. This is because, in the first cycle of charge/discharge, Li_2O was stripped from the Li_2MnO_3 component of LRNMC to form MnO_2 at this potential. This reaction is irreversible.[34,35] This process is also the reason for oxygen release in the main structure of LRNMC to form a spinel-like phase.[36] Compared with LRNMC, the peak intensity of 1F1Al-LRNMC was significantly smaller, indicating that during the first cycle of charge/discharge, the AlF_3-Al_2O_3 coating effectively suppressed the occurrence of this irreversible reaction.

Furthermore, the reversible redox peak at lower than 3 V can be attributed to the lithiation/delithiation of the spinel structure of MnO_2.[37,38] After the second cycle, the peak intensity at this position increased, indicating that a transition from a layered structure to a spinel structure occurred during the cycling process. Compared with LRNMC, the peak intensity of 1F1Al-LRNMC was smaller, which indicates that the coating layer inhibited the process of layered LRNMC transforming into spinel during the charge/discharge cycling. A similar phenomenon can also be found from the first cycle charge/discharge profile as shown in Figure 4d. Although the same discharge capacity was delivered, the charging capacity of the first cycle of 1F1Al-LRNMC was much smaller than that of LRNMC. All of the results indicate that the AlF_3-Al_2O_3 coating suppressed the O_2 release of LRNMC during the first cycle of charge/discharge, thereby alleviating the subsequent phase

https://doi.org/10.1021/acsami.1c20005
ACS Appl. Mater. Interfaces 2022, 14, 3991−4003

transition of the layered structure, which contributed to the cycling stability of coated LRNMC.

To further investigate the reason for the electrochemical performance improvement, electrochemical impedance spectra (EIS) of half cells made of LRNMC, 2Al-LRNMC, and 1F1Al-LRNMC particles, respectively, were collected after 0, 20, 50, and 100 cycles of charge/discharge, as shown in Figure 5. To

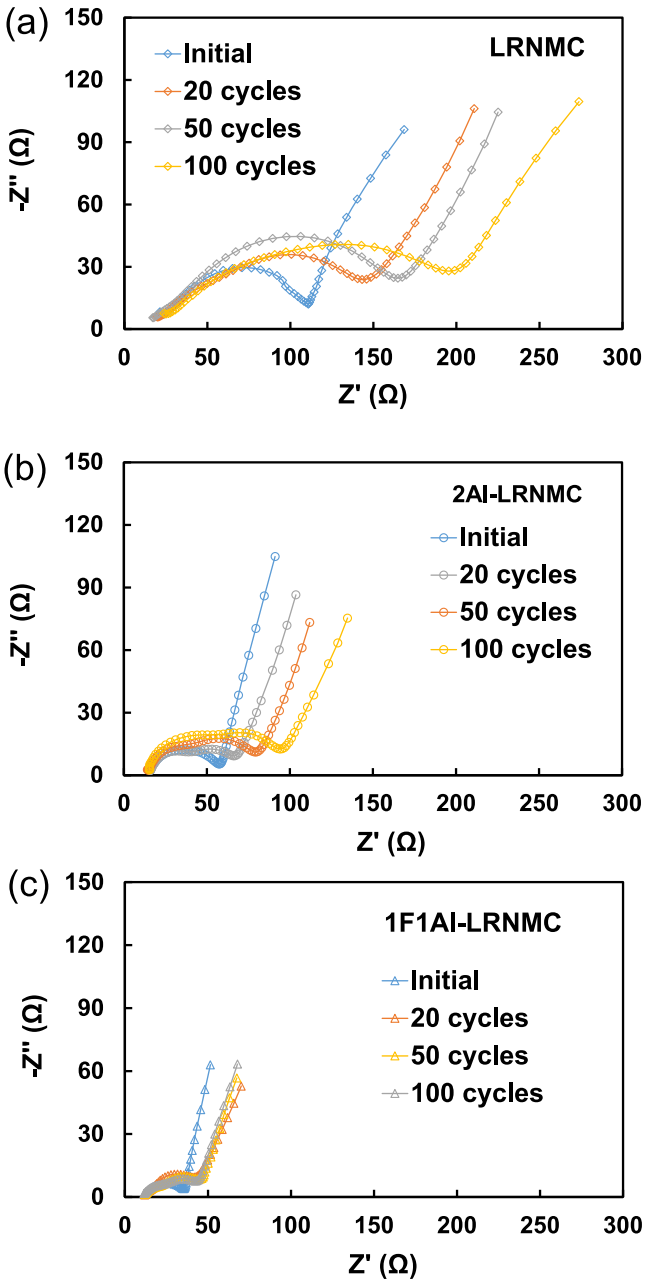

Figure 5. Electrochemical impedance spectroscopy profiles of half cells made of (a) LRNMC, (b) 2Al-LRNMC, and (c) 1F1Al-LRNMC particles after 0, 20, 50, and 100 cycles of charge/discharge.

obtain the specific resistance value, we performed a fitting on the obtained results using the fitted equivalent circuit, as shown in Figure S2. Table S1 shows all calculated values. In the fitting circuit, R_f represents the impedance of the surface film at high frequencies of 100−10 kHz, and R_{ct} represents the impedance generated by the charge transfer reaction in the middle-frequency range of the 10 kHz to 10 Hz region.

For LRNMC, R_{ct} gradually increased along with the cycling number (as shown in Figure 5a), which indicates that the decomposition of electrolyte and the deposition of byproducts on the electrode surface have been accompanied during the cycling process, and these byproducts were not conducive to Li ions, which led to the gradual increase of R_{ct}. The EIS of 2Al-LRNMC (Figure 5b) show very small R_{ct} and R_f at the beginning, which indicates that an ultrathin Al_2O_3 film was beneficial to the charge transfer at the interface. However, during the cycling process, R_{ct} also exhibited a gradual increase, although the increase was much lower than that of LRNMC, which indicates that Al_2O_3 suppressed interface side reactions and deposition of byproducts to a certain extent. 1F1Al-LRNMC presented a smaller R_{ct} and R_f; after 20 cycles of charge/discharge, R_{ct} remained almost unchanged, as shown in Figure 5c. This indicates that a stable interfacial layer was formed on the surface of LRNMC, which was conducive to the charge transfer, and effectively suppressed the occurrence of side reactions between electrode and electrolyte.

Characterization of Cycled Electrodes. Similar to the anode, which forms a solid electrolyte interphase (SEI) on the surface of electrode to prevent the co-embedding of solvent molecules and avoid the damage to the electrode material caused by the co-embedding of solvent molecules,[39] a CEI is also formed on the cathode surface along with the decomposition of electrolyte during the cycling process. This CEI also plays a vital role in the performance of cathode.[40,41] The results of electrochemical impedance spectroscopy indicate that the AlF_3-Al_2O_3 coating on LRNMC was conducive to a robust and conductive CEI. Therefore, figuring out the composition of CEI is the key to understanding the mechanism by which the AlF_3-Al_2O_3 coating improves the electrochemical performance of LRNMC. Therefore, scanning electron microscopy (SEM) and XPS were performed to analyze the surface morphology and compositions of CEI on cathode electrodes after charge/discharge cycling.

As shown in Figure 6, all of the fresh electrodes (Figure 6a−c) look similar, indicating that the surface coating on LRNMC particles did not change the bulk structure of fabricated electrodes. In contrast, the morphology of LRNMC, 2Al-LRNMC, and 1F1Al-LRNMC electrodes changed extensively after 100 cycles of charge/discharge. As shown in Figure 6d,g, the particles on the LRNMC electrode became larger and rougher, which can be attributed to the formation of CEI. Cycled 2Al-LRNMC showed a rough surface and enlarged particles too, as shown in Figure 6e,h, but the surface was smoother compared to that of the cycled LRNMC electrode, indicating a different morphology of CEI. For the cycled 1F1Al-LRNMC electrode, features of the fresh electrode can still be observed, as shown in Figure 6f,i; there was some deposit on the surface, but the amount of deposit was significantly lesser than that of the other two. The SEM results show that CEI was formed on all electrode surfaces after charge/discharge cycling, but the amount of deposit and the morphology were completely different, indicating that AlF_3-Al_2O_3 coating inhibited the decomposition of electrolyte and changed the composition of CEI as well.

XPS was used to reveal the components of CEI on all cycled electrodes after 100 cycles of charge/discharge. The C 1s spectra of fresh and cycled LRNMC, 2Al-LRNMC, and 1F1Al-LRNMC electrodes were collected, as displayed in Figure 7a−c. The height of peaks is directly related to the frequency of a given bond on the surface. Since the surface coating was

https://doi.org/10.1021/acsami.1c20005
ACS Appl. Mater. Interfaces 2022, 14, 3991−4003

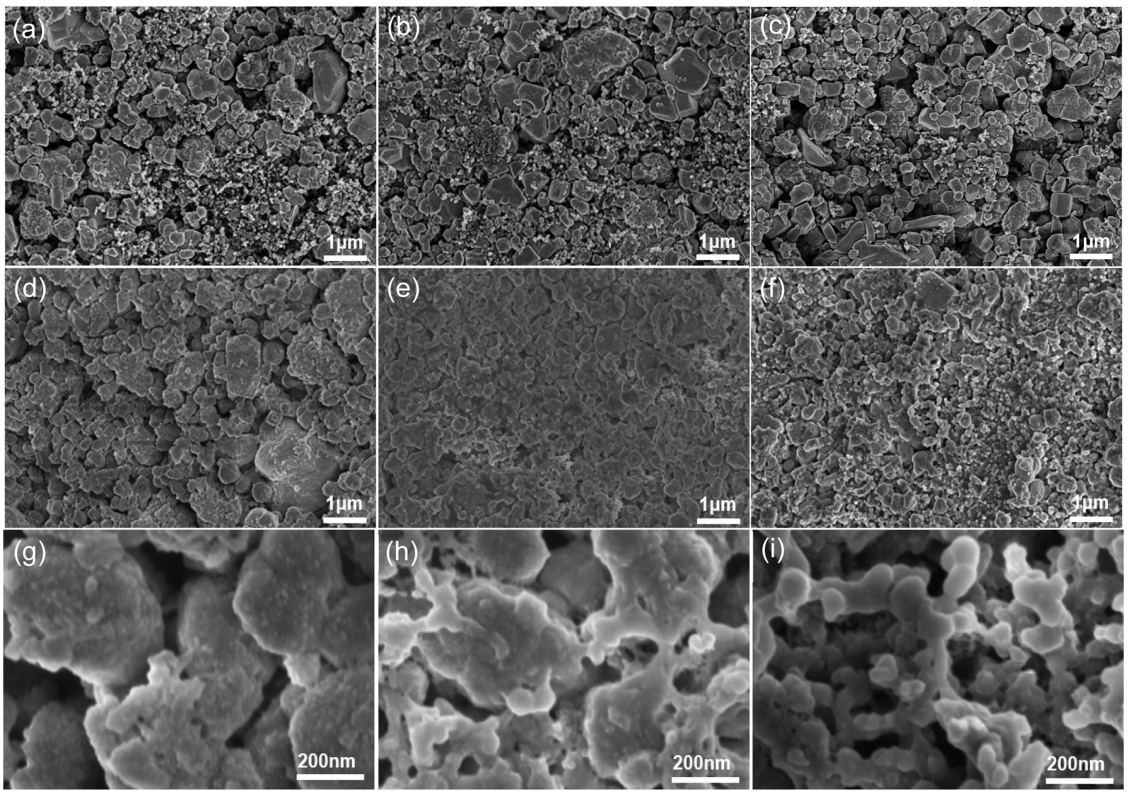

Figure 6. SEM images of fresh electrodes made of (a) LRNMC, (b) 2Al-LRNMC, and (c) 1F1Al-LRNMC particles and cycled electrodes made of (d, g) LRNMC, (e, h) 2Al-LRNMC, and (f, i) 1F1Al-LRNMC particles. All cycled electrodes were charged/discharged for 100 cycles.

ultrathin, there was no significant difference between all of these three fresh electrodes in the C 1s core level. The C 1s spectra of all fresh electrodes can be deconvoluted into several components, with C−C species at 284.6 eV and C−O species at 286.1 eV, which belongs to adventitious carbon.[42,43] A pair of peaks with a similar area at 290.8 and 286.4 eV belonged to $-CF_2$ and $-CH_2$, which is from poly(vinylidene fluoride) (PVDF) added as the binder.

After charge/discharge cycling, the most obvious change of the surface compositions of electrodes was from the peak intensity of the C−O bond. The C−O bond can be derived from the organic components attached to the electrode surface after the electrolyte is decomposed. Based on the intensity change of C−O bonds from cycled LRNMC to cycled 1F1Al-LRNMC, it can be concluded that in the half cell fabricated from LRNMC, the organic solvent in the electrolyte is decomposed during the cycling process, and the decomposed organic components, such as R−O−Li, are deposited on the surface of LRNMC electrode. The degree of decomposition and deposition in the half cell fabricated from 2Al-LRNMC was less than that of the LRNMC half cell, and the organic carbon component observed from C 1s of the 1F1Al-LRNMC electrode was very small, indicating that the decomposition of the solvent was effectively suppressed in the half cell fabricated from 1F1Al-LRNMC. CO_3^{2-} at 289.3 eV normally results from the reaction of released O_2 and electrolyte on the electrode surface during the cycling process. A weaker peak of CO_3^{2-} for the cycled electrode fabricated from 1F1Al-LRNMC indicates that AlF_3-Al_2O_3 coating can reduce the release of oxygen, thereby alleviating the subsequent decomposition of the electrolyte. This also indicates that the extent of organic deposition on the surface of the 1F1Al-LRNMC electrode is much lower than that on LRNMC and 2Al-LRNMC electrodes.

The O 1s spectra of cycled LRNMC, cycled 2Al-LRNMC, and cycled 1F1Al-LRNMC electrodes are shown in Figure 7d−f. For uncoated LRNMC, the main peak at 529.8 eV belonged to the lattice oxygen bonded to transition metals. After Al_2O_3 coating, the signal of Al−O at 531.1 eV could be detected on the surface of 2Al-LRNMC and 1F1Al-LRNMC, and another signal of 532.3 eV could be attributed to Al−O−H; the existence of −O−H was due to the introduction of water precursor during the ALD process.[44] As Al_2O_3 ALD was applied on both 2Al-LRNMC and 1F1Al-LRNMC, they both exhibited almost the same O 1s spectrum. After charge/discharge cycling, the ratio of lattice oxygen of all three electrodes was significantly lower, indicating that CEI was formed in all three electrodes, but the compositions of the CEI layer on the surface of the three electrodes were different. On the surface of LRNMC, the components of O 1s mainly included R−O−Li species (531.6 eV), $-CO_3$ species (532.8 eV), and $Li_xPO_yF_z$ species (533.7 eV);[45] among these three components, the proportion of R−O−Li was 61%, which indicates that the organic component accounted for the main proportion in the generated CEI layer. On the surface of 2Al-LRNMC and 1F1Al-LRNMC, the ratio of organic components in the CEI layer was significantly smaller. Combined with the C 1s XPS results of cycled 1F1Al-LRNMC, it can be concluded that there was still a very weak decomposition of organic solvents of the electrolyte during the cycling process; however, compared to the uncoated LRNMC, this side reaction was effectively suppressed.

Figure S3a,b shows the F 1s spectra of fresh LRNMC and 1F1Al-LRNMC electrodes. Due to the small content of AlF_3

https://doi.org/10.1021/acsami.1c20005
ACS Appl. Mater. Interfaces 2022, 14, 3991−4003

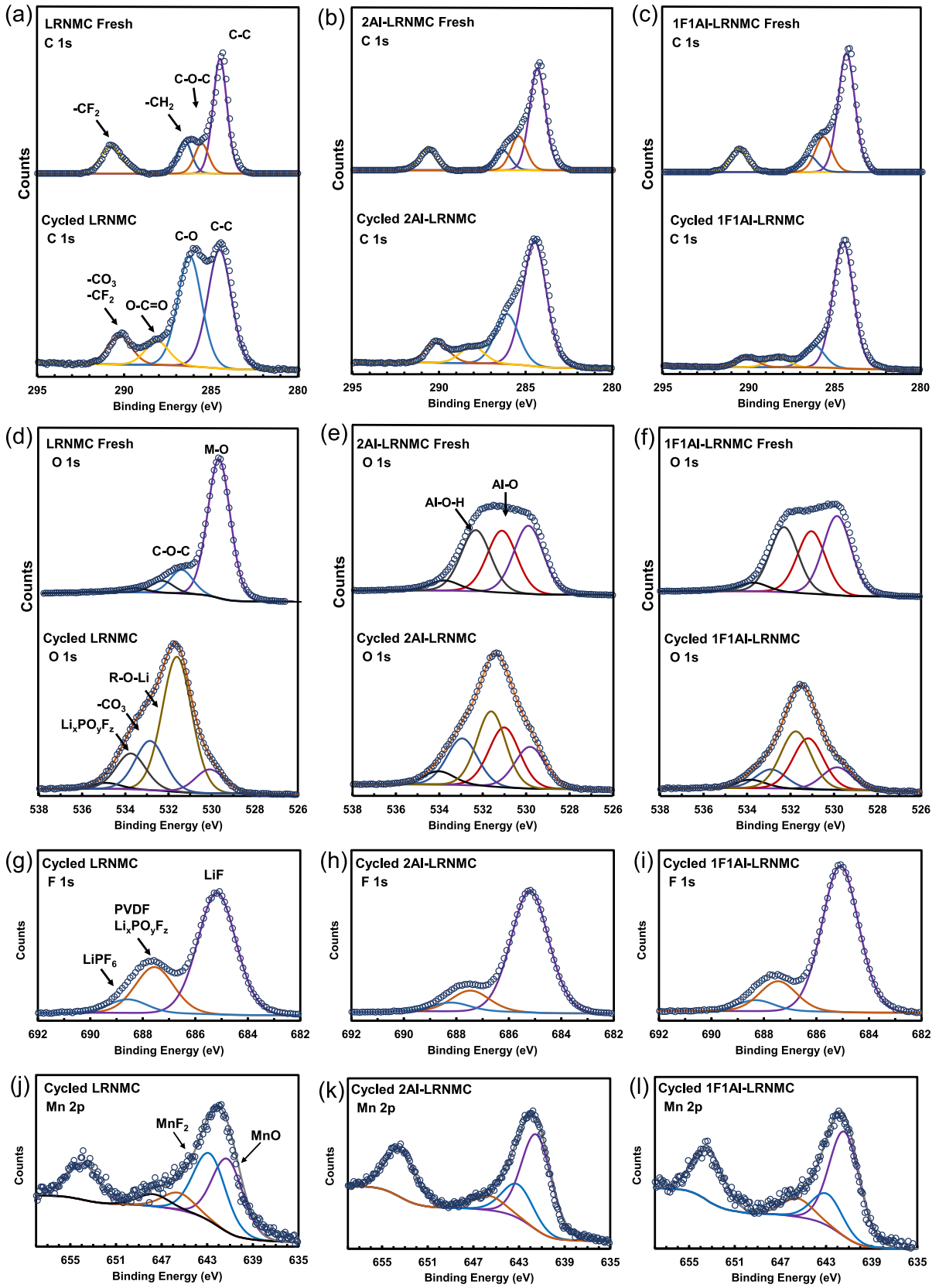

Figure 7. XPS C 1s spectra of fresh and cycled electrodes made of (a) LRNMC, (b) 2Al-LRNMC, and (c) 1F1Al-LRNMC particles. O 1s spectra of fresh and cycled electrodes made of (d) LRNMC, (e) 2Al-LRNMC, and (f) 1F1Al-LRNMC particles. F 1s spectra of cycled electrodes made of (g) LRNMC, (h) 2Al-LRNMC, and (i) 1F1Al-LRNMC particles. Mn 2p spectra of cycled electrodes made of (j) LRNMC, (k) 2Al-LRNMC, and (l) 1F1Al-LRNMC particles. All cycled electrodes were charged/discharged for 100 cycles.

https://doi.org/10.1021/acsami.1c20005
ACS Appl. Mater. Interfaces 2022, 14, 3991−4003

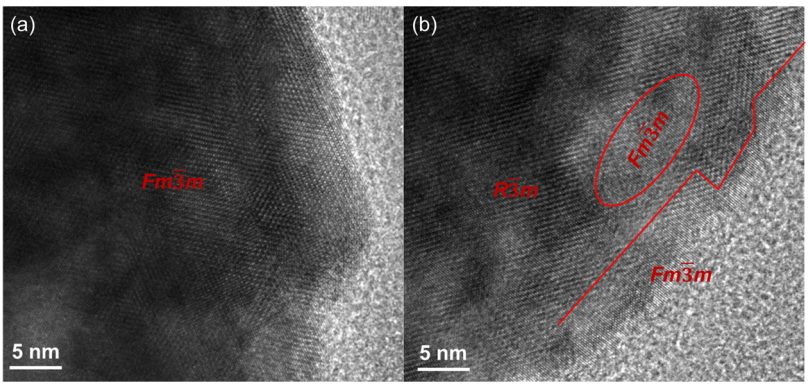

Figure 8. HRTEM images of (a) LRNMC and (b) 1F1Al-LRNMC particles from cycled electrodes.

from the ALD coating and the 10% mass ratio of PVDF added as a binder, both these electrodes showed similar F 1s spectra. The strong peak at 687.7 eV belonged to $-CF_2$ in PVDF, and there was a small peak that belonged to LiF (685.2 eV). The existence of LiF on the fresh electrodes could be due to the slight decomposition of PVDF during electrode fabrication.

Figure 7g–i shows the F 1s spectra of cycled LRNMC, cycled 2Al-LRNMC, and cycled 1F1Al-LRNMC electrodes. Due to the formation of the CEI layer, the peak of $-CF_2$ in PVDF was obviously weakened, and it almost overlapped the peak position of $Li_xPO_yF_z$ (687.5 eV). The XPS results of F 1s can be used to analyze the inorganic components in the CEI layer. After cycling, all of the three electrodes showed the same compositions. The main composition was LiF, which was generated from the reaction between Li_2O released from LRNMC during the first charging process and HF generated by decomposition of $LiPF_6$ from electrolyte or PVDF and a small amount of $LiPF_6$ (688.5 eV) from the electrolyte.[46,47]

Figure S3c–f shows the results of Al 2p of 2Al-LRNMC and 1F1Al-LRNMC before and after charge/discharge cycling. The surface of LRNMC showed a peak belonging to AlF_3 (76.2 eV), and the content was high. In contrast, the content of 1F1Al-LRNMC was still very low. During the cycling process, Al_2O_3 on the surface of 2Al-LRNMC was gradually corroded by HF, while the Al_2O_3 film with AlF_3 overcoating was well protected.

Figure 7j–l shows the Mn 2p spectra of cycled LRNMC, cycled 2Al-LRNMC, and cycled 1F1Al-LRNMC electrodes. Two main components could be deconvoluted from Mn 2p spectra of all cycled electrodes: MnO at 641.4 eV and MnF_2 at 642.8 eV.[48,49] MnO belonged to the rock-salt phase due to the phase transformation, and MnF_2 was generated due to the dissolution of Mn^{3+}.[50,51] For cycled LRNMC, the ratio of MnF_2 was 50.8%, which indicates that during the cycling process, a large amount of Mn^{3+} was corroded by HF generated by the decomposition of the electrolyte. Compared to this, the MnF_2 ratios of cycled 2Al-LRNMC and cycled 1F1Al-LRNMC are 26.6 and 23.1%, respectively, indicating that the surface coating effectively inhibited the corrosion of active materials by HF, thereby alleviating the dissolution of Mn^{3+}.

HRTEM analysis was carried out to investigate the phase transition of LRNMC and 1F1Al-LRNMC after 100 cycles of charge/discharge. As shown in Figure 8a, after cycling, LRNMC exhibited an increase in the rock-salt phase ($Fm\bar{3}m$), and a larger area of layered phase ($R\bar{3}m$) transformed into the rock-salt phase. In contrast, for cycled 1F1Al-LRNMC (Figure 8b), the thickness of the rock-salt phase increased slightly, and a small inner area of the layered phase transformed into rock-salt phase, as circled in Figure 8b, which indicates that the AlF_3-Al_2O_3 coating can suppress phase transition efficiently during the cycling process.

Combined with the obtained electrochemical performance and the analysis of the morphology and composition of the CEI layer by SEM and XPS, it can be concluded that during the cycling process of the LRNMC-based half cells, the decomposition products of the organic solvent and the inorganic components in the electrolyte are deposited on the surface of the electrode material to form an interfacial layer, which leads to the gradual increase of the interfacial resistance and, thus, the gradual decrease in electrochemical performance. Although the Al_2O_3 coating suppressed the decomposition of organic solvents to a certain extent and improved the cycle stability of the material, the organic components in the CEI still hindered the transport of Li ions and affected the rate performance of LRNMC. The coating of AlF_3-Al_2O_3 could effectively inhibit the decomposition and deposition of organic components, thereby forming a dense inorganic protective layer made of Al_2O_3, AlF_3, and LiF on the surface of the electrode material, as schematically shown in Figure 9. This

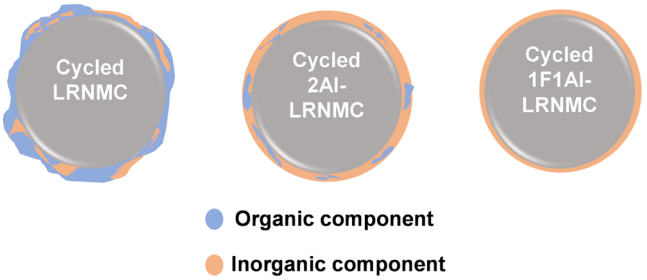

Figure 9. Schematic representation of the components of the CEI layer on the surface of cycled LRNMC, cycled 2Al-LRNMC, and cycled 1F1Al-LRNMC.

inorganic CEI was more robust and conducive to Li ions, and it could inhibit further interfacial reactions, thereby improving the charge/discharge capacity and cycling stability of LRNMC.

Long-Term Protection of AlF_3-Al_2O_3 Coating. We noticed an unusual phenomenon during the electrochemical testing. All of the coated LRNMC-based half cells suddenly dropped sharply after charge/discharge to a certain number of cycles. Our hypothesis was that this could be due to the dead lithium fully covered on the surface of the Li anode, which

https://doi.org/10.1021/acsami.1c20005
ACS Appl. Mater. Interfaces 2022, 14, 3991–4003

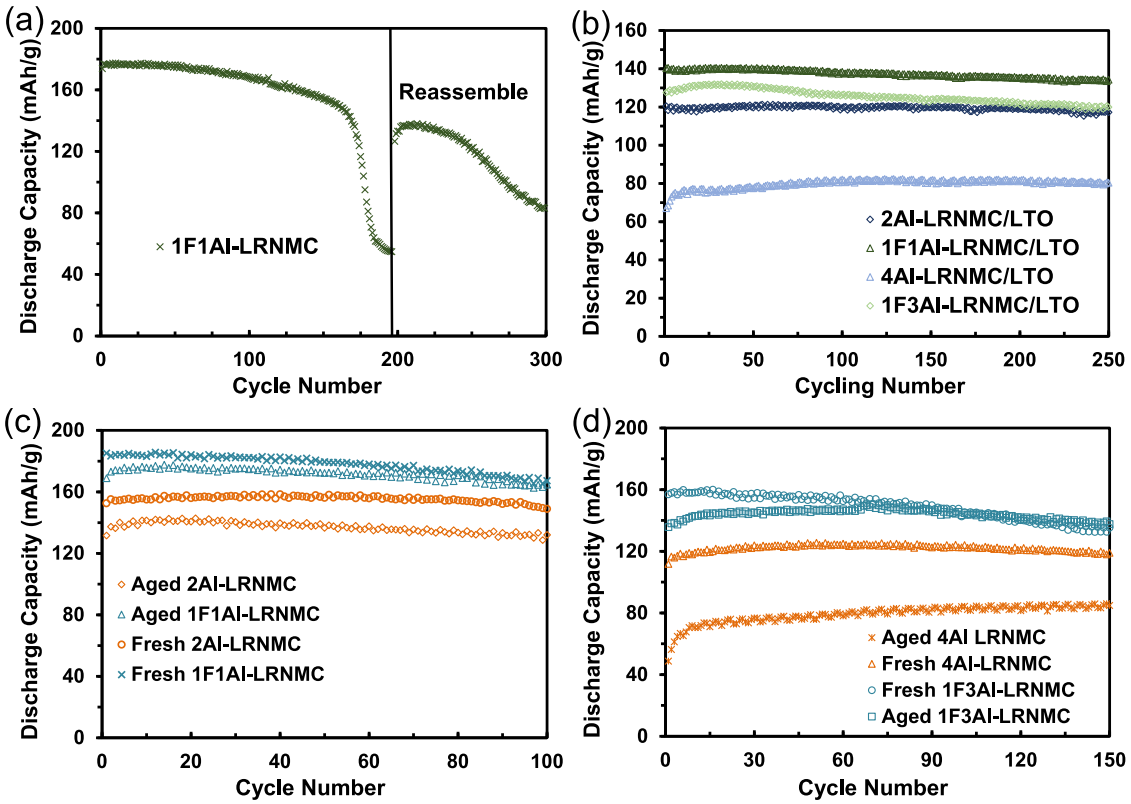

Figure 10. (a) Cycling performance of disassembled and reassembled 1F1Al-LRNMC. (b) Discharge performance of full cells based on Al_2O_3-coated LRNMC, AlF_3-Al_2O_3-coated LRNMC, and $Li_4Ti_5O_{12}$ at a 1C rate. Cycling performance of half cells based on (c) fresh and aged 1F1Al-LRNMC and 2Al-LRNMC and (d) fresh and aged 1F3Al-LRNMC and 4Al-LRNMC.

resulted in the failure of the anode. To verify this, we disassembled a 1F1Al-LRNMC-based half cell after 200 cycles of charge/discharge, removed the electrode, replaced it with a new lithium foil, and tested the electrochemical performance of the reassembled half cell again. The electrochemical performance was restored before its failure, as shown in Figure 10a. This experiment indirectly proved that the degradation of the electrochemical performance was caused by the consumption of the lithium electrode to some extent and not the failure of cathode material. Therefore, to fully study the cycling stability of modified LRNMC, $Li_4Ti_5O_{12}$ (LTO) was selected as anode material instead of lithium metal. A series of LRNMC/LTO coin cells were assembled. Figure 10b shows the discharge performance of these coin cells. It can be seen that all full cells delivered excellent cycling stability. The full cell based on 1F1Al-LRNMC/LTO showed the best discharge capacity.

Most reported research of surface treatment has focused on the immediate effects of improving electrochemical performance. To the best of our knowledge, no one has reported whether the surface coating can remain on the surface of materials for a long time and whether the coating can still provide the same effect after a long period of storage. In this study, all coated materials were stored in a dry container for over 1 year. XPS and EDS mapping were applied to investigate whether the coating could remain on the surface of LRNMC particles after a long time of storage. As shown in Figure S4, there is no obvious difference between the XPS results of aged 1F1Al-LRNMC and freshly coated 1F1Al-LRNMC particles. From the results of EDS mapping (Figure S5), the coating is still well distributed on the surface of LRNMC particles. Electrodes, made of electrode materials after long-time storage, were labeled aged LRNMC. Half cells based on these aged materials were assembled. Figure 10c,d shows the discharge performance of aged $2Al_2O_3$ and aged $1AlF_3$-$1Al_2O_3$-coated LRNMC for up to 100 cycles of charge/discharge. After over 1 year, the aged $2Al_2O_3$ LRNMC sample exhibited an obvious capacity decrease; in contrast, the $1AlF_3$-$1Al_2O_3$ sample delivered the same electrochemical performance as that of the fresh $1AlF_3$-$1Al_2O_3$-coated LRNMC. The results of this series of experiments indicate that the fluorinated Al_2O_3 film has better durability during long-term storage.

CONCLUSIONS

In short, an ultrathin film composed of AlF_3 and Al_2O_3 was coated on LRNMC particles by ALD in a fluidized bed reactor. This coating provided effective protection for the cathode material from the erosion of electrolyte, suppressed side reactions between the electrolyte and the electrode, decreased the dissolution of transition metal ions, and inhibited the transformation of the layered phase to a spinel phase. Compared with pristine LRNMC, the electrochemical performance of 1F1Al-LRNMC was significantly improved. SEM and XPS analyses of cycled electrodes indicated that AlF_3-Al_2O_3 coating could effectively inhibit the decomposition of the electrolyte during the charge/discharge cycling process, thereby changing the composition of the CEI layer and forming a protective layer that was more conducive to Li ion transport and cycling stability. Moreover, the coated material had 100% repeatability of the electrochemical performance after storing over 1 year, while the performance of Al_2O_3 ALD coated LRNMC or pristine LRNMC significantly decreased, indicating that this AlF_3-Al_2O_3 coating can provide protection

https://doi.org/10.1021/acsami.1c20005
ACS Appl. Mater. Interfaces 2022, 14, 3991−4003

for long-term cycling stability and long-term shelf life. This strategy can be applied to other types of electrode materials to help improve the performance of LIBs, enabling them to have higher output voltage, higher energy density, and longer service life.

EXPERIMENTAL SECTION

Atomic Layer Deposition. ALD thin-film coating on LRNMC particles was carried out in a fluidized bed reactor. The precursors were trimethylaluminum (TMA) (Sigma-Aldrich) and H_2O for Al_2O_3 ALD and TMA and HF-pyridine (Sigma-Aldrich) for AlF_3 ALD. For a typical Al_2O_3 ALD cycle, TMA was first fed into the reactor and reacted with functional groups on the particle substrate surface. When the surface reaction was completed, TMA feeding into the reactor was stopped and an inert gas such as nitrogen gas was used to remove the unreacted TMA and any byproducts from the reactor system. Next, water was introduced into the reactor, which stripped the methyl groups from the adsorbed TMA and left a hydroxide group on the substrate surface. By repeating this process, we can coat a thin film with precisely controlled thicknesses on the surface of the particles. A similar approach was used for AlF_3 ALD. All precursors were fed into the reactor using their room-temperature vapor pressures as driving force, and the reaction temperature was 150 °C.

Coin Cell Assembly. To fabricate an electrode sheet, LRNMC, Super P (Alfa Aesar), and PVDF (Alfa Aesar) were mixed according to a mass ratio of LRNMC/Super P/PVDF = 80:10:10. *N*-methyl-2-pyrrolidine (NMP) (Sigma-Aldrich) was used as a solvent. Typical loading of the active cathode material of one electrode was about 3.5 mg/cm^2. LIB coin cells were assembled in a dry glovebox filled with argon. For half cells, Li foil was used as the anode, and the battery model was a CR2032-type button coin cell. For full cell, LTO was used as the anode. Further, 1.0 M $LiPF_6$ in a mixture solvent of EC and DMC (EC/DMC = 1:1 in volume) (Sigma-Aldrich) was used as the electrolyte. A trilayer polymer film made of polypropylene (PP)/polyethylene (PE)/PP (Celgard Inc.) was used as the separator.

Electrochemical Testing. Galvanostatic charge/discharge cycling was carried out on a battery workstation (Neware Corp.) at room temperature with a current density of 1C (1C = 250 mA/g). A current density of 0.1C was applied for formation in the first two cycles. The potential range was from 2.0 to 4.8 V (vs Li/Li^+). CV and electrochemical impedance spectroscopy tests were carried out using an SP-150 potentiostat. EIS were collected over a frequency range from 1 MHz to 1 mHz with an amplitude of 5 mV after cells were fully discharged.

Material Characterizations. SEM imaging was used to analyze the surface morphology of fresh and cycled LRNMC electrodes using an FEI Helios Nano Lab 600 FESEM. A Kratos 165 XPS scanning microprobe (Physical Electronics) was applied to analyze surface compositions of the coated LRNMC particles and cycled LRNMC electrodes. The transmission electron microscope (FEI Tecnai F30 G2 Twin) was operated at 300 kV to measure the thickness of coating films for AlF_3-Al_2O_3-coated LRNMC. Scanning TEM-EDS mapping was performed with a Bruker 30 mm^2 active area silicon drift detector with a super light element window to confirm the elemental distribution.

ASSOCIATED CONTENT

Supporting Information

The Supporting Information is available free of charge at https://pubs.acs.org/doi/10.1021/acsami.1c20005.

XPS spectra of survey scan and Al 2p of Al_2O_3 ALD coated LRNMC particles (Figure S1); equivalent circuit model of LRNMC-based lithium-ion battery (Figure S2); XPS spectra of F 1s of fresh electrodes made of LRNMC and 1F1Al-LRNMC particles and Al 2p of fresh and cycled electrodes made of 2Al-LRNMC and 1F1Al-LRNMC particles (Figure S3); XPS spectra of survey scan of fresh and aged 1F1Al-LRNMC particles (Figure S4); EDS mapping of Ni, Mn, Co, and Al of aged 1F1Al-LRNMC particles (Figure S5); and R_f and R_{ct} values of electrodes made of LRNMC, 1F1Al-LRNMC, and 2Al-LRNMC, respectively, before cycling and after charge/discharge for 100 cycles (Table S1) (PDF)

AUTHOR INFORMATION

Corresponding Author

Xinhua Liang − *Linda and Bipin Doshi Department of Chemical and Biochemical Engineering, Missouri University of Science and Technology, Rolla, Missouri 65409, United States;* orcid.org/0000-0001-7979-0532; Email: liangxin@mst.edu

Authors

Han Yu − *Linda and Bipin Doshi Department of Chemical and Biochemical Engineering, Missouri University of Science and Technology, Rolla, Missouri 65409, United States*

Xiaoqing He − *Electron Microscopy Core Facility, University of Missouri, Columbia, Missouri 65211, United States; Department of Mechanical and Aerospace Engineering, University of Missouri, Columbia, Missouri 65211, United States*

Complete contact information is available at: https://pubs.acs.org/10.1021/acsami.1c20005

Notes

The authors declare the following competing financial interest(s): A U.S. PCT application (application number US2020/032,299), with X.L. and H.Y. as co-inventors, has been filed by Missouri University of Science and Technology.

ACKNOWLEDGMENTS

This work was supported in part by the National Science Foundation, United States [grant NSF DMR 1464111] and Linda and Bipin Doshi endowment of Missouri University of Science and Technology. The authors thank Dr. Clarissa Wisner at Materials Research Center at Missouri University of Science and Technology for SEM analysis.

REFERENCES

(1) Dunn, B.; Kamath, H.; Tarascon, J.-M. Electrical Energy Storage for The Grid: A Battery of Choices. *Science* **2011**, *334*, 928−935.

(2) Lu, L.; Han, X.; Li, J.; Hua, J.; Ouyang, M. A Review on The Key Issues for Lithium-Ion Battery Management in Electric Vehicles. *J. Power Sources* **2013**, *226*, 272−288.

(3) Qiu, B.; Zhang, M.; Xia, Y.; Liu, Z.; Meng, Y. S. Understanding and Controlling Anionic Electrochemical Activity in High-Capacity Oxides for Next Generation Li-Ion Batteries. *Chem. Mater.* **2017**, *29*, 908−915.

(4) Yan, J.; Liu, X.; Li, B. Recent Progress in Li-Rich Layered Oxides as Cathode Materials for Li-Ion Batteries. *RSC Adv.* **2014**, *4*, 63268−63284.

(5) Yan, P.; Nie, A.; Zheng, J.; Zhou, Y.; Lu, D.; Zhang, X.; Xu, R.; Belharouak, I.; Zu, X.; Xiao, J. Evolution of Lattice Structure and Chemical Composition of The Surface Reconstruction Layer in $Li_{1.2}Ni_{0.2}Mn_{0.6}O_2$ Cathode Material for Lithium Ion Batteries. *Nano Lett.* **2015**, *15*, 514−522.

(6) Yan, P.; Zheng, J.; Zhang, X.; Xu, R.; Amine, K.; Xiao, J.; Zhang, J.-G.; Wang, C.-M. Atomic to Nanoscale Investigation of Functionalities of An Al_2O_3 Coating Layer on A Cathode For Enhanced Battery Performance. *Chem. Mater.* **2016**, *28*, 857−863.

(7) Sathiya, M.; Abakumov, A. M.; Foix, D.; Rousse, G.; Ramesha, K.; Saubanère, M.; Doublet, M. L.; Vezin, H.; Laisa, C. P.; Prakash, A. S.; et al. Origin of Voltage Decay in High-Capacity Layered Oxide Electrodes. *Nat. Mater.* **2015**, *14*, 230−238.
(8) Jacquet, Q.; Iadecola, A.; Saubanère, M.; Li, H.; Berg, E. J.; Rousse, Gl.; Cabana, J.; Doublet, M.-L.; Tarascon, J.-M. Charge Transfer Band Gap as An Indicator of Hysteresis in Li-Disordered Rock Salt Cathodes for Li-Ion Batteries. *J. Am. Chem. Soc.* **2019**, *141*, 11452−11464.
(9) Xiao, B.; Sun, X. Surface and Subsurface Reactions of Lithium Transition Metal Oxide Cathode Materials: An Overview of The Fundamental Origins and Remedying Approaches. *Adv. Energy Mater.* **2018**, *8*, No. 1802057.
(10) Yang, P.; Zheng, J.; Kuppan, S.; Li, Q.; Lv, D.; Xiao, J.; Chen, G.; Zhang, J.-G.; Wang, C.-M. Phosphorus Enrichment as A New Composition in The Solid Electrolyte Interphase of High-Voltage Cathodes and Its Effects on Battery Cycling. *Chem. Mater.* **2015**, *27*, 7447−7451.
(11) Imhof, R.; Novák, P. Oxidative Electrolyte Solvent Degradation in Lithium-Ion Batteries: An In Situ Differential Electrochemical Mass Spectrometry Investigation. *J. Electrochem. Soc.* **1999**, *146*, 1702−1706.
(12) Erickson, E. M.; Li, W.; Dolocan, A.; Manthiram, A. Insights into The Cathode-Electrolyte Interphases of High-Energy-Density Cathodes in Lithium-Ion Batteries. *ACS Appl. Mater. Interfaces* **2020**, *12*, 16451−16461.
(13) Li, T.; Yuan, X.-Z.; Zhang, L.; Song, D.; Shi, K.; Bock, C. Degradation Mechanisms and Mitigation Strategies Of Nickel-Rich NMC-Based Lithium-Ion Batteries. *Electrochem. Energy Rev.* **2020**, *3*, 43−80.
(14) Guan, P.; Zhou, L.; Yu, Z.; Sun, Y.; Liu, Y.; Wu, F.; Jiang, Y.; Chu, D. Recent Progress of Surface Coating on Cathode Materials for High-Performance Lithium-Ion Batteries. *J. Energy Chem.* **2020**, *43*, 220−235.
(15) Liu, J.; Sun, X. Elegant Design of Electrode and Electrode/Electrolyte Interface in Lithium-Ion Batteries by Atomic Layer Deposition. *Nanotechnology* **2014**, *26*, No. 024001.
(16) Meng, X. Towards High-Energy and Durable Lithium-Ion Batteries Via Atomic Layer Deposition: Elegantly Atomic-Scale Material Design and Surface Modification. *Nanotechnology* **2014**, *26*, No. 020501.
(17) Liang, X.; Hakim, L. F.; Zhan, G. D.; McCormick, J. A.; George, S. M.; Weimer, A. W.; Spencer, J. A.; Buechler, K. J.; Blackson, J.; Wood, C. J.; et al. Novel Processing to Produce Polymer/Ceramic Nanocomposites by Atomic Layer Deposition. *J. Am. Ceram. Soc.* **2007**, *90*, 57−63.
(18) Leskelä, M.; Ritala, M. Atomic Layer Deposition (ALD): from Precursors to Thin Film Structures. *Thin Solid Films* **2002**, *409*, 138−146.
(19) Richards, W. D.; Miara, L. J.; Wang, Y.; Kim, J. C.; Ceder, G. Interface Stability in Solid-State Batteries. *Chem. Mater.* **2016**, *28*, 266−273.
(20) Jain, A.; Ong, S. P.; Hautier, G.; Chen, W.; Richards, W. D.; Dacek, S.; Cholia, S.; Gunter, D.; Skinner, D.; Ceder, G.; et al. Commentary: The Materials Project: A Materials Genome Approach to Accelerating Materials Innovation. *APL Mater.* **2013**, *1*, No. 011002.
(21) Tiurin, O.; Solomatin, N.; Auinat, M.; Ein-Eli, Y. Atomic Layer Deposition (ALD) of Lithium Fluoride (LiF) Protective Film on Li-Ion Battery $LiMn_{1.5}Ni_{0.5}O_4$ Cathode Powder Material. *J. Power Sources* **2020**, *448*, No. 227373.
(22) Xie, H.; Liang, Z.; Luo, D.; Zhang, Y.; Ding, X.; Cui, J.; Zhang, Z.; Lin, Z. A General Route of Fluoride Coating on The Cyclability Regularity of High-Voltage NCM Cathodes. *Chem. Commun.* **2020**, *56*, 12009−12012.
(23) Xie, J.; Sendek, A. D.; Cubuk, E. D.; Zhang, X.; Lu, Z.; Gong, Y.; Wu, T.; Shi, F.; Liu, W.; Reed, E. J.; et al. Atomic Layer Deposition of Stable $LiAlF_4$ Lithium Ion Conductive Interfacial Layer for Stable Cathode Cycling. *ACS Nano* **2017**, *11*, 7019−7027.
(24) Wang, S.; Bai, Q.; Nolan, A. M.; Liu, Y.; Gong, S.; Sun, Q.; Mo, Y. Lithium Chlorides and Bromides as Promising Solid-State Chemistries for Fast Ion Conductors with Good Electrochemical Stability. *Angew. Chem., Int. Ed.* **2019**, *58*, 8039−8043.
(25) Jin, Y.; Yu, H.; Liang, X. Understanding The Roles of Atomic Layer Deposition in Improving The Electrochemical Performance of Lithium-Ion Batteries. *Appl. Phys. Rev.* **2021**, *8*, No. 031301.
(26) Hoskins, A. L.; McNeary, W. W.; Millican, S. L.; Gossett, T. A.; Lai, A.; Gao, Y.; Liang, X.; Musgrave, C. B.; Weimer, A. W. Nonuniform Growth of Sub-2 Nanometer Atomic Layer Deposited Alumina Films on Lithium Nickel Manganese Cobalt Oxide Cathode Battery Materials. *ACS Appl. Nano Mater.* **2019**, *2*, 6989−6997.
(27) Kim, J. W.; Kim, D. H.; Oh, D. Y.; Lee, H.; Kim, J. H.; Lee, J. H.; Jung, Y. S. Surface Chemistry of $LiNi_{0.5}Mn_{1.5}O_4$ Particles Coated by Al_2O_3 Using Atomic Layer Deposition for Lithium-Ion Batteries. *J. Power Sources* **2015**, *274*, 1254−1262.
(28) Xie, J.; Zhao, J.; Liu, Y.; Wang, H.; Liu, C.; Wu, T.; Hsu, P.-C.; Lin, D.; Jin, Y.; Cui, Y. Engineering The Surface of $LiCoO_2$ Electrodes Using Atomic Layer Deposition for Stable High-Voltage Lithium Ion Batteries. *Nano Res.* **2017**, *10*, 3754−3764.
(29) Yu, H.; Gao, Y.; Liang, X. Slightly Fluorination of Al_2O_3 ALD Coating on $Li_{1.2}Mn_{0.54}Co_{0.13}Ni_{0.13}O_2$ Electrodes: Interface Reaction to Create Stable Solid Permeable Interphase Layer. *J. Electrochem. Soc.* **2019**, *166*, A2021−A2027.
(30) Jung, Y. S.; Cavanagh, A. S.; Riley, L. A.; Kang, S. H.; Dillon, A. C.; Groner, M. D.; George, S. M.; Lee, S. H. Ultrathin Direct Atomic Layer Deposition on Composite Electrodes for Highly Durable And Safe Li-Ion Batteries. *Adv. Mater.* **2010**, *22*, 2172−2176.
(31) Xiao, Y.; Wang, Y.; Bo, S.-H.; Kim, J. C.; Miara, L. J.; Ceder, G. Understanding Interface Stability in Solid-State Batteries. *Nat. Rev. Mater.* **2020**, *5*, 105−126.
(32) Gu, M.; Belharouak, I.; Zheng, J.; Wu, H.; Xiao, J.; Genc, A.; Amine, K.; Thevuthasan, S.; Baer, D. R.; Zhang, J.-G.; et al. Formation of The Spinel Phase in The Layered Composite Cathode Used in Li-Ion Batteries. *ACS Nano* **2013**, *7*, 760−767.
(33) Mohanty, D.; Sefat, A. S.; Kalnaus, S.; Li, J.; Meisner, R. A.; Payzant, E. A.; Abraham, D. P.; Wood, D. L.; Daniel, C. Investigating Phase Transformation in The $Li_{1.2}Co_{0.1}Mn_{0.55}Ni_{0.15}O_2$ Lithium-Ion Battery Cathode During High-Voltage Hold (4.5 V) Via Magnetic, X-Ray Diffraction and Electron Microscopy Studies. *J. Mater. Chem. A* **2013**, *1*, 6249−6261.
(34) Johnson, C. S.; Li, N.; Lefief, C.; Vaughey, J. T.; Thackeray, M. M. Synthesis, Characterization and Electrochemistry of Lithium Battery Electrodes: $xLi_2MnO_3\cdot(1-x)LiMn_{0.333}Ni_{0.333}Co_{0.333}O_2$ ($0\leq x\leq 0.7$). *Chem. Mater.* **2008**, *20*, 6095−6106.
(35) Kim, J.-S.; Johnson, C.; Vaughey, J.; Thackeray, M. Pre-Conditioned Layered Electrodes for Lithium Batteries. *J. Power Sources* **2006**, *153*, 258−264.
(36) Strehle, B.; Kleiner, K.; Jung, R.; Chesneau, F.; Mendez, M.; Gasteiger, H. A.; Piana, M. The Role of Oxygen Release From Li-and Mn-Rich Layered Oxides During The First Cycles Investigated by On-Line Electrochemical Mass Spectrometry. *J. Electrochem. Soc.* **2017**, *164*, A400−A406.
(37) Huang, Y.; Dong, Y.; Li, S.; Lee, J.; Wang, C.; Zhu, Z.; Xue, W.; Li, Y.; Li, J. Lithium Manganese Spinel Cathodes for Lithium-Ion Batteries. *Adv. Energy Mater.* **2021**, *11*, No. 2000997.
(38) Thackeray, M.; Croy, J. R.; Lee, E.; Gutierrez, A.; He, M.; Park, J. S.; Yonemoto, B. T.; Long, B. R.; Blauwkamp, J. D.; Johnson, C. S.; et al. The Quest for Manganese-Rich Electrodes for Lithium Batteries: Strategic Design and Electrochemical Behavior. *Sustainable Energy Fuels* **2018**, *2*, 1375−1397.
(39) An, S. J.; Li, J.; Daniel, C.; Mohanty, D.; Nagpure, S.; Wood, D. L., III The state of Understanding of The Lithium-Ion-Battery Graphite Solid Electrolyte Interphase (SEI) and Its Relationship to Formation Cycling. *Carbon* **2016**, *105*, 52−76.
(40) Balasubramanian, M.; Lee, H. S.; Sun, X.; Yang, X.-Q.; Moodenbaugh, A.; McBreen, J.; Fischer, D. A.; Fu, Z. Formation of SEI on Cycled Lithium-Ion Battery Cathodes: Soft X-Ray Absorption Study. *Electrochem. Solid-State Lett.* **2002**, *5*, No. A22.

https://doi.org/10.1021/acsami.1c20005
ACS Appl. Mater. Interfaces 2022, 14, 3991−4003

(41) Ostrovskii, D.; Ronci, F.; Scrosati, B.; Jacobsson, P. A FTIR and Raman Study of Spontaneous Reactions Occurring at The $LiNi_yCo_{(1-Y)}O_2$ Electrode/Non-Aqueous Electrolyte Interface. *J. Power Sources* **2001**, *94*, 183−188.
(42) Wu, B.; Ren, Y.; Mu, D.; Liu, X.; Yang, G.; Wu, F. Effect of Lithium Carbonate Precipitates on The Electrochemical Cycling Stability of $LiCoO_2$ Cathodes at A High Voltage. *RSC Adv.* **2014**, *4*, 10196−10203.
(43) Zheng, J.; Yan, P.; Mei, D.; Engelhard, M. H.; Cartmell, S. S.; Polzin, B. J.; Wang, C.; Zhang, J. G.; Xu, W. Highly Stable Operation of Lithium Metal Batteries Enabled by The Formation of A Transient High-Concentration Electrolyte Layer. *Adv. Energy Mater.* **2016**, *6*, No. 1502151.
(44) Fang, R.-C.; Sun, Q.-Q.; Zhou, P.; Yang, W.; Wang, P.-F.; Zhang, D. W. High-Performance Bilayer Flexible Resistive Random Access Memory Based on Low-Temperature Thermal Atomic Layer Deposition. *Nanoscale Res. Lett.* **2013**, *8*, No. 92.
(45) Lim, J.-H.; Myung, Y.; Yang, M.; Lee, J.-w. Facile Formation of A LiF-Carbon Layer as An Artificial Cathodic Electrolyte Interphase Through Encapsulation of A Cathode with Carbon Monofluoride. *ACS Appl. Mater. Interfaces* **2021**, *13*, 31741−31748.
(46) Lu, Y.-C.; Mansour, A. N.; Yabuuchi, N.; Shao-Horn, Y. Probing The Origin of Enhanced Stability of "$AlPO_4$" Nanoparticle Coated $LiCoO_2$ During Cycling to High Voltages: Combined XRD and XPS Studies. *Chem. Mater.* **2009**, *21*, 4408−4424.
(47) Veluchamy, A.; Doh, C.-H.; Kim, D.-H.; Lee, J.-H.; Shin, H.-M.; Jin, B.-S.; Kim, H.-S.; Moon, S.-I. Thermal Analysis of Li_xCoO_2 Cathode Material of Lithium Ion Battery. *J. Power Sources* **2009**, *189*, 855−858.
(48) Mansour, A. N.; Kwabi, D. G.; Quinlan, R. A.; Lu, Y.-C.; Shao-Horn, Y. Probing the Electrode-Electrolyte Interface in Cycled $LiNi_{0.5}Mn_{1.5}O_4$ by XPS Using Mg and Synchrotron X-Rays. *J. Electrochem. Soc.* **2016**, *163*, A2911−A2918.
(49) Huang, Y.; Ding, R.; Ying, D.; Shi, W.; Huang, Y.; Tan, C.; Sun, X.; Gao, P.; Liu, E. Engineering Doping-Vacancy Double Defects and Insights Into The Conversion Mechanisms of An Mn−O−F Ultrafine Nanowire Anode for Enhanced Li/Na-Ion Storage and Hybrid Capacitors. *Nanoscale Adv.* **2019**, *1*, 4669−4678.
(50) Benedek, R.; Thackeray, M. Reaction Energy for $LiMn_2O_4$ Spinel Dissolution in Acid. *Electrochem. Solid-State Lett.* **2006**, *9*, No. A265.
(51) Park, O. K.; Cho, Y.; Lee, S.; Yoo, H.-C.; Song, H.-K.; Cho, J. Who Will Drive Electric Vehicles, Olivine or Spinel? *Energy Environ. Sci.* **2011**, *4*, 1621−1633.

https://doi.org/10.1021/acsami.1c20005
ACS Appl. Mater. Interfaces 2022, 14, 3991−4003